Journal of Bio- and Tribo-Corrosion (2020) 6:41
https://doi.org/10.1007/s40735-020-00338-x

Electrochemical Studies and the Surface Examination of Low Carbon Steel by Applying the Extract of *Citrus sinensis*

Akhil Saxena[1] · Vishal Sharma[1] · Kamal Kishor Thakur[1] · Nishant Bhardwaj[2]

Received: 4 October 2019 / Revised: 7 January 2020 / Accepted: 18 February 2020 / Published online: 2 March 2020

Abstract
The corrosion inhibition effect of *citrus sinensis* belonging to Rutaceae family has been analyzed on the low carbon steel corrosion in 0.5 M H_2SO_4 by using weight reduction estimations and electrochemical measurements. It is observed that the extract of *Citrus sinensis* acts like a mixed type corrosion inhibitor and its inhibition effectiveness increases on increasing the concentration. The best inhibition effect of the *Citrus sinensis* extract for low carbon steel in 0.5 M H_2SO_4 was obtained at 500 mg/L concentration. Further the Langmuir adsorption isotherm was used to check the adsorption behavior of the extract on the metal surface. The surface morphology of the low carbon steel is also studied by using scanning electron microscopy and atomic force microscopy.

Keywords *Citrus sinensis* · Low carbon steel · Weight reduction · FTIR · SEM · Quantum calculations

1 Introduction

Low carbon steel is used to make a broad assortment of equipments and metallic structures because of its low cost and easy availability. A remarkable economic loss is caused during the cleaning of boilers, pickling of low carbon steel in industry because strong acids containing compounds are generally used as pickling agents or to remove undesirable surface stores from the metal surface [1]. Because of the aggressive behavior of the acid solutions, inhibitors are used to reduce the acidic assault on metallic materials. All through the past decades, some modern inhibitors are incorporated and utilized successfully to inhibit the corrosion of low carbon steel [2]. Anyway the most significant disadvantage related with the vast majority of these inhibitors is that they are not eco-friendly and are venomous and costly. Accordingly the investigation of the most recent non-dangerous or low poisonous corrosion inhibitors is imperative to overcome this downside. The examination in the field of eco-friendly corrosion inhibitors has been carried out towards the objective of exploitation of low cost, successful inhibitors at low or zero natural effect. The synthetic inhibitors may have some negative results for nature and they may likewise be hurtful to human wellbeing [3]. Lately, the investigation of modest, eco-friendly and biodegradable corrosion inhibitors is getting more consideration. To overcome this problem, the trend is going towards the development of corrosion inhibitors by using the waste materials of fruits, like their peels, or some weed and medicinal plants which have already been tested for their medicinal uses but their corrosion inhibition properties are not investigated yet. They can be considered in the form of the natural inhibitors and can be adsorbed on the metal surface by forming a chemical bond with the metal (chemical adsorption), or physically adsorbed or sometimes it may be a combination of both. The extract of these plant materials or peels of fruits has several compounds with the tendency to adsorb on the metal surface. This region of research is of much significance on the grounds that, notwithstanding being naturally well disposed and biologically adequate, plant items are reasonable, promptly accessible and inexhaustible wellsprings of materials. Some previous researchers have reported the efficiency of plant materials as corrosion inhibitors, such as: the extract of *Kola nitida shows* 78% efficiency at 1200 mg/L inhibitor

✉ Akhil Saxena
akhil.uis@cumail.in

[1] Department of Chemistry, University Institute of Sciences, Chandigarh University, Gharuan, Mohali, Punjab 140413, India

[2] Department of Chemistry, Lovely Professional University Punjab, Phagwara, India

concentration [4], 81% inhibition efficiency is observed at 4000 mg/L concentration for *Phyllanthus amarus* extract [5], *Radish* extract shows 79% efficiency at 10 ml/100 ml [6], *Eleusine aegyptiaca* extract shows 87% efficiency at 1800 mg/L concentration [7], *Henna* extract shows 67% efficiency at 1000 mg/L concentration [8], 88% efficiency is observed at 1500 mg/L concentration for *Artemisia pallens* extract [9], *Mangrove* extract shows 88% efficiency at 3000 mg/L concentration [10], *Salvia officinalis* extract shows 86% efficiency at 1000 mg/L concentration [11], *Pimenta dioica* extract shows 86% efficiency at 500 ppm [12], watermelon extract is observed to show 77% efficiency at 200 ppm [13], *Neolamarckia cadamba* extract shows 88% efficiency at 500 ppm [14], *Spondias mombin* extract shows 86% efficiency at 500 ppm [15], *Dendrocalmus sinicus* extract shows 78% efficiency at 200 ppm [16]. Through these examinations understood that the corrosion inhibition effect of the plant extract is because of the existence of natural species like tannins, alkaloids, sugars, amino acids, and proteins. These natural compounds contain polar capacities with N, O heteroatoms further as conjugated double bonds or aromatic rings in their molecular structures which are the significant adsorption sites. The objective of the present work is to investigate the corrosion inhibition properties and the adsorption behavior of *C. sinensis* extract. It is an Indian plant usually known as Orange. Although the medicinal activities of *C. sinensis* have been investigated earlier, but they do not explore this plant extract as a corrosion inhibitor. We have already found that the extract of *C. sinensis* comprises of Ascorbic acid, flavonoids and some other compounds as shown in Fig. 1 [17]. Here the corrosion inhibition performance is checked by using the weight reduction process and the electrochemical measurements. The modification in the surface morphology was then further studied with SEM and AFM studies.

2 Experimental

2.1 Specimen Preparation

The composition of the low carbon steel used in this work is shown in Table 1. The low carbon steel samples were given a dimensions of 1 cm^2 by mechanical cutting. Then the surface of all the low carbon steel coupons was cleaned with silicon carbide papers of different grades (100, 200, 500, and 1000) before the corrosion test.

2.2 Corrosive Medium and the Plant Extract

In the present examination, tests were carried out in 0.5 M H_2SO_4 solution, which was prepared in double-distilled water using AR grade sulfuric acid provided by Sigma chemicals. In weight loss studies, the volume of 0.5 M H_2SO_4 was kept 100 ml and for electrochemical estimations, 250 ml of 0.5 M H_2SO_4 was utilized. The peels of the *C. sinensis* are shown in Fig. 2.

The peels of the *C. sinensis* were washed, dried, and converted into powdered form by grinding the plant material. Then 50 g of the powdered sample was refluxed with 250 ml ethanol at 75 °C for about 24 h. The solution was then filtered and dried on a water bath, which finally gave 4.5 g darker strong store. The *C. sinensis* extract was then diluted with sulfuric acid to prepare test solutions of different

Table 1 Composition of the low carbon steel

S. No.	Metal	Amount (%)
1.	Iron	97.60
2.	Carbon	0.083
3.	Phosphorous	0.12
4.	Chromium	0.45
5.	Nickle	0.27
6.	Copper	0.43

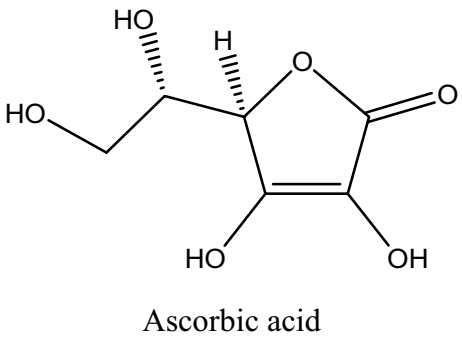

Fig. 1 Chemical constituent of *C. sinensis*

Fig. 2 Peels of *C. sinensis*

concentrations (100, 200, 300, 400, 500 mg/L). The maximum solubility of the *C. sinensis* extract in 0.5 M H_2SO_4 was observed up to 500 mg/L.

2.3 Weight Reduction Measurements

Here, the volume of the corrosive solution used for weight reduction experiments was kept 100 ml. So here, we immersed the low carbon steels of 1 cm^2 dimensions in the corrosive medium for 24 h. The low carbon steel coupons were weighted accurately before and after immersing them from the corrosive medium. Triplicate tests were performed for every sample of low carbon steel. The following equations were used to determine the weight loss data.

$$CR = \frac{\Delta W}{D \times A \times T} \times 87600 \tag{1}$$

$$\theta = \frac{w_0 - w_i}{w_0} \tag{2}$$

$$\eta\% = \frac{w_0 - w_i}{w_0} \times 100 \tag{3}$$

where, W → weight loss (mg).

A → area of low carbon steel coupon (cm^2).

T → immersion time.

D → density of low carbon steel (g cm^{-3}).

w_0 and w_i → the weight reduction in the absence and presence of the inhibitor.

2.4 Adsorption Isotherm

Reliable facts were observed regarding the relation between plant material and the low carbon steel on studying the adsorption isotherms. A decrease in corrosion rate on utilization of inhibitors is either by obstructing the cathodic reaction rate or by preventing the anodic metal dissolution or both by adsorbing on the metal surface in the corrosive medium [18–20]. Seiverts et al. showed a relationship between inhibitor concentration and inhibition efficiency [21]. It uses most ordinarily the Langmuir adsorption isotherm [22]. The surface coverage (Θ) for various concentrations of inhibitors in 0.5 M H_2SO_4 solution was tried graphically to fit a reasonable adsorption isotherm. Langmuir adsorption isotherm can be written in the form [23]

$$\frac{C}{\theta} = \frac{1}{K_{ads}} + C \tag{4}$$

where, C is the concentration of inhibitor and K_{ads} is the adsorption constant.

2.5 Corrosion Inhibition Studies by Potentiodynamic Polarization

The polarization estimations were completed at 298 K utilizing a three-electrode system. The volume of the corrosive medium for polarization studies was kept 250 ml. The mild steel coupons were immersed in Araldite resin in such a way that it leaves an area (1 cm^2) and hence it is the working electrode. Initially, the working electrode was kept undisturbed in the corrosive medium for 60 min to settle the OCP. Polarization plots were obtained at a scan rate of 1 mV/s between potentials of − 250 mV and + 250 mV. A platinum electrode was used as a counter electrode and a saturated calomel electrode as the reference electrode [12, 24–27]. The polarization parameters were calculated using the following equations- [28].

$$\eta(\%) = \frac{I_{0corr} - I_{icorr}}{I_{0corr}} \times 100 \tag{5}$$

where, I_{0corr} and I_{icorr} represent the corrosion current density in the absence and presence of the inhibitor, respectively.

2.6 Corrosion Inhibition Studies by Electrochemical Impedance Spectroscopy (EIS)

The same electrochemical cell and electrochemical workstation, as specified for polarization estimations, was used to carry out electrochemical impedance spectroscopy estimations in the frequency range from 100 kHz to 0.01 Hz using amplitude of 5 mV at OCP. Just like to that of the polarization measurements, the working electrode was kept undisturbed in the corrosive medium for about 60 min. The impedance information was obtained by using the Nyquist and Bode plots [29]. The EIS parameters were calculated from the following equation-

$$\eta(\%) = \frac{R_{ct} - R^0_{ct}}{R_{ct}} \times 100 \tag{6}$$

where, R_{ct} → charge transfer resistance at individual concentration of inhibitor.

R^0_{ct} → charge transfer resistance at zero concentration of inhibitor.

2.7 FTIR Spectroscopy

The Fourier transform infrared spectroscopic analysis is a standout amongst the most essential methods for elucidation of the phenomenon of adsorbed inhibitor molecules. The infrared spectral information has been considered by many specialists as an immediate evidence of the presence of inhibitors on the metal surface [30–32]. In the present study, we performed Fourier transform infrared

spectroscopic analysis to show the existence of functional groups containing heteroatoms. The *C. sinensis* extract blended with KBr was transferred into a pallet for FTIR characterization. The FTIR spectra of the *C. sinensis* extract were recorded in the range 500–4000 cm^{-1} by using a FTIR 8400S spectrophotometer.

2.8 UV–Visible Spectroscopy

With the help of the Shimadzu UV-1800 absorption spectrophotometer, the UV spectra of the corrosive solution (before and after the corrosion test) were taken. Both these spectra were contrasted to explain the inhibition mechanism.

2.9 Surface Studies

The surface morphology of the exposed metal surface has been explained widely by many specialists to comprehend the idea of surface products got in the absence and presence of inhibitors [33–36]. Here, the changes in the surface morphology of low carbon steel were observed by taking the SEM and AFM images of low carbon steel in three different environments. First of all the SEM and AFM images were taken for the non-corroded steel coupon (finely cleaned low carbon steel), then for the corroded coupon (steel coupon dipped in the corrosive medium), and finally for the inhibited steel coupon (steel coupon dipped in the corrosive medium with inhibitor). The SEM and AFM images of the low carbon steel were taken by using LEO435BP and NT-MDT-INTEGRA, respectively. These SEM and AFM images were then compared with each other to explain the possible adsorption of inhibitor on the metal surface.

2.10 Quantum Chemical Study

The quantum chemical estimations were done using Hyperchem 8.0 programming with the DFT method. Here we determined the energy of the highest occupied molecular orbital (E_{HOMO}) and the lowest unoccupied molecular orbital (E_{LUMO}).The reactivity of a chemical species is very much characterized as far as frontier orbitals; the highest occupied molecular orbital (HOMO) and the lowest unoccupied molecular orbitals (LUMO) [37, 38]. The energy difference between the HOMO and LUMO can be determined by using the following equation-

$$\Delta E = E_{LUMO} - E_{HOMO} \tag{7}$$

3 Results and Discussion

3.1 Weight Reduction Analysis

The corrosion inhibition efficiency (η %), corrosion rate (CR) and surface coverage (Θ) at various concentrations (100–500 mg/L) of *C. sinensis* extract as obtained by weight loss method have been reported in Table 2. From Table 2, it is clear that on increasing the inhibitor concentration, the corrosion rate decreases and the

Table 2 Corrosion rate and inhibition efficiency at different concentrations of *C. sinensis* extract

Temperature (K)	Concentration of inhibitor (mg/L)	Weight loss (mg cm^{-2} h^{-1})	Efficiency (η %)	Surface coverage (θ)	Corrosion rate (CR) (mm/Y)
298	0	0.0563	0	0	26.11
	100	0.0101	82.06	0.8206	4.68
	200	0.0078	86.14	0.8614	3.61
	300	0.0059	89.52	0.8952	2.73
	400	0.0037	93.07	0.9307	1.80
	500	0.0019	96.62	0.9662	0.88
308	0	0.0894	0	0	41.46
	100	0.0201	77.51	0.7751	9.32
	200	0.0156	82.55	0.8255	7.23
	300	0.0120	86.57	0.8657	5.56
	400	0.0090	89.93	0.8993	4.17
	500	0.0064	92.84	0.9284	2.96
318	0	0.1356	0	0	62.88
	100	0.0352	74.04	0.7404	16.32
	200	0.0281	79.27	0.7927	13.03
	300	0.0221	83.70	0.8370	10.24
	400	0.0196	85.54	0.8554	9.09
	500	0.0147	89.15	0.8915	6.81

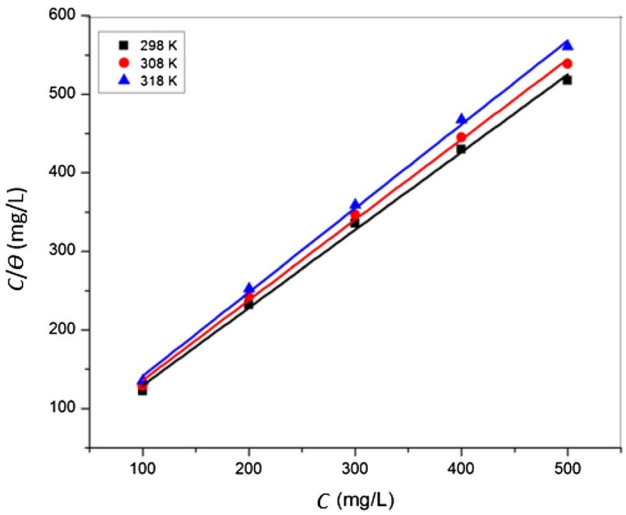

Fig. 3 Langmuir adsorption isotherm for *C. sinensis* on low carbon steel in 0.5 M H_2SO_4

Table 3 Adsorption parameters for mild steel in 0.5 M H_2SO_4 at optimum concentration of *C. sinensis* inhibitor

Temperature (K)	K_{ads} (Lmg^{-1})	Slope	R^2
298	57.17	0.98	0.9972
308	25.93	1.02	0.9981
318	16.43	1.06	0.9981

inhibition efficiency increases. This is because when inhibitor adsorbs on the metal surface, then it forms a protective layer on the metal surface, which reduces the corrosion reaction [39]. Here we analyzed the inhibition effectiveness of the *C. sinensis* extract in the temperature range of 298–318 K. It is observed that on increasing the temperature, the inhibition efficiency decreases. It happens because the pre adsorbed inhibitor molecules starts detaching from the metal surface on increasing the temperature.

3.2 Adsorption Isotherm

The plots of C/Θ vs. C for the *C. sinensis* extract as showed by the Langmuir adsorption isotherm equation are shown in Fig. 3. The estimation of K_{ads} was computed from the intercept of Fig. 3 and is detailed in Table 3. Table 3 shows that the slope value is 1 at all the studied temperatures, which shows that the inhibitor is being adsorbed on the surface of the metal efficiently. Also, a decrease in the values of the adsorption equilibrium constant is observed with increasing temperature, which suggests the desorption of adsorbed inhibitor molecules at increasing temperature.

3.3 Potentiodynamic Polarization Studies

In the first phase of electrochemical measurements we have conducted the polarization measurements for which we have recorded the values of some of the important corrosion parameters like corrosion potential (E_{corr}), corrosion current density (I_{corr}), anodic and cathodic Tafel slopes (β_a and β_c) and inhibition efficiency (η %). These parameters have been reported in Table 4 and the polarization curves are shown in Fig. 4. The corrosion current densities were determined by extrapolation of straight parts of anodic and cathodic bends to the point of convergence of the relating corrosion potential. The Tafel bends indicates decrease in the current densities of the anodic and cathodic branches in the presence of *C. sinensis* extract. The discovered improvement is additionally the aftereffects of covering of adsorbed inhibitor molecules on the low carbon steel surface and diminishing disintegration of steel surface zone. The Tafel plot also indicates that the *C. sinensis* extract is able to affect both the reactions of anodic metal dissolution and cathodic hydrogen evolution, when it is added to the corrosive medium. It is reported previously that if the changes in the values of E_{corr} for the individual concentration of inhibitor corresponding to the zero concentration of inhibitor lies between 85 mV, then the inhibitor is considered as a combine type (i.e., both anodic and cathodic) corrosion inhibitor. Therefore, in the present work, this change in E_{corr} values is only 69 mV. So, accordingly, the inhibitor here can be considered to act like a mix type inhibitor [40]. It can also be explained on behalf of the

Table 4 Polarization parameters for mild steel in 0.5 M H_2SO_4 without and with different concentrations of *C. sinensis* extract

Inhibitor concentration (mg/L)	E_{corr} (V vs. SCE)	I_{corr} (A cm^{-2})	β_a (V/dec)	β_c (V/dec)	Efficiency (η %)
0	−0.465	0.0008909	141.66	164.25	0
100	−0.454	0.0001687	48.56	127.05	81.06
200	−0.471	0.0001161	49.01	117.45	86.96
300	−0.460	0.0001069	48.19	117.08	88.01
400	−0.456	0.00008020	45.94	114.61	90.09
500	−0.534	0.00005816	49.97	106.21	93.47

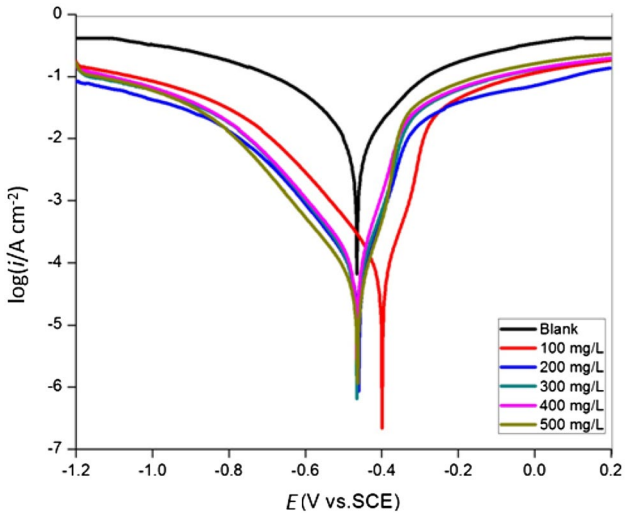

Fig. 4 Polarization curves for low carbon steel in 0.5 M H_2SO_4 at different concentrations of *C. sinensis* extract

values of anodic and cathodic Tafel slopes i.e., β_a and β_c. On moving from 0 to 100 mg/L, it is clear that the change in the value of β_c is less than the change in β_a. So at this point the inhibitor is acting like an anodic inhibitor. Further on moving from 100 to 200 mg/L, the change in value of β_a is less than β_c. So here the inhibitor is considered to be a cathodic inhibitor. Overall, we observed that on some concentrations, the inhibitor is acting like an anodic inhibitor and for others, it is acting like a cathodic inhibitor. This is the reason because of which we consider the present inhibitor as a mix type corrosion inhibitor that can protect metal from corrosion either by reducing the anodic reaction or cathodic reaction. In this work, the inhibitor shows maximum corrosion inhibition efficiency at 500 mg/L with an inhibition efficiency of 93.47%.

3.4 Electrochemical Impedance Spectroscopy (EIS) Studies

For electrochemical analysis, the working electrode was kept undisturbed for 60 min in the corrosive medium so that the OCP would be set. The Nyquist and Bode plots for low carbon steel are shown in Fig. 5, and the corresponding EIS parameters are reported in Table 5. The circuit shown in Fig. 6 is a parallel combination of charge transfer resistance (R_{ct}) and the constant phase element (CPE). It helps to analyze the EIS spectra. The Nyquist plot shows that, as we are moving to the higher concentration of inhibitor, the diameter of the semi-circle increases with each concentration which is in the agreement of advancing the inhibition effect of inhibitor. This incrementation in R_{ct} is because of the development of a defensive film at the metal interface. The changes in R_{ct} and CPE values are because of the substitution of water

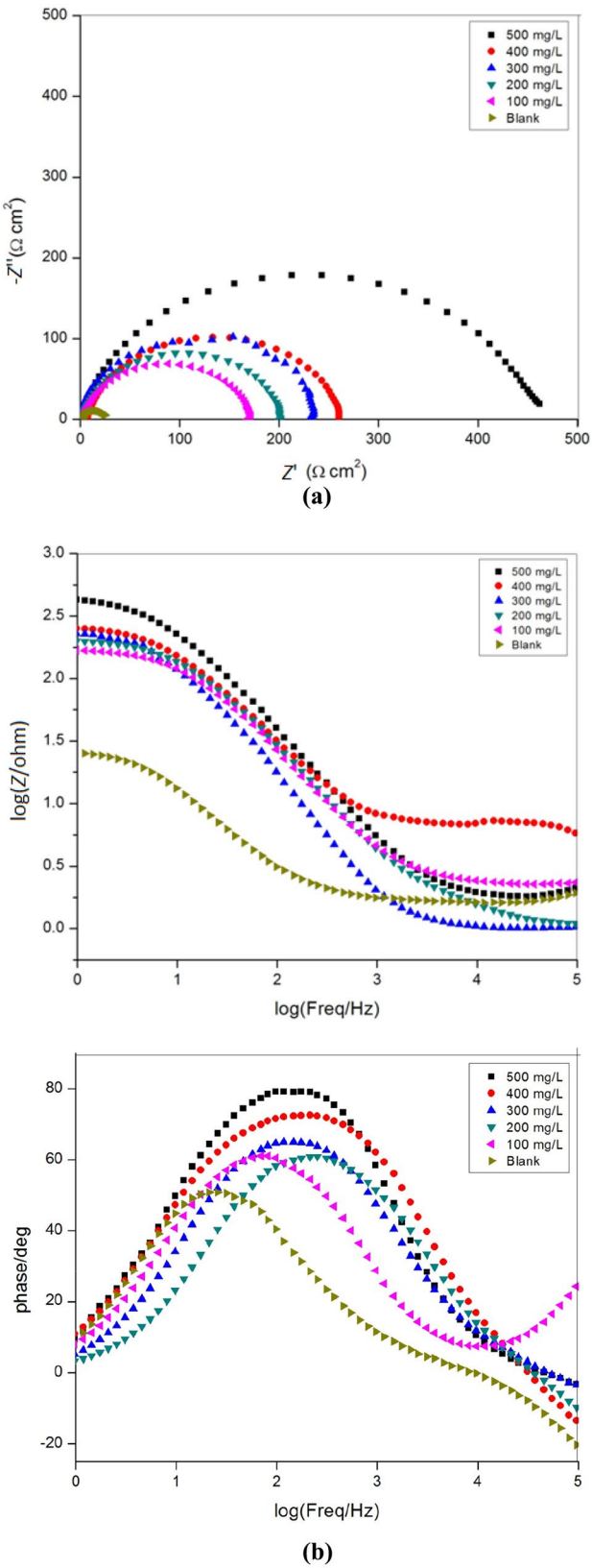

Fig. 5 Nyquist **a** and Bode **b** plots for MS in 0.5 M H_2SO_4 without and with various concentrations of *Citrus sinensis* extract at 298 K

Table 5 EIS parameters for low carbon steel in 0.5 M H_2SO_4 at different concentrations of *Citrus sinensis* extract

Acid solution	Concentration of inhibitor (mg/L)	R_{ct} (Ω cm^2)	*CPE* (μF cm^{-2})	Efficiency (η %)
0.5 M H_2SO_4	0	25.164	1.3×10^{-3}	0
	100	172.17	9.7×10^{-5}	85.38
	200	201.56	9.4×10^{-5}	87.51
	300	235.42	7.4×10^{-5}	89.31
	400	260.55	6.7×10^{-5}	90.34
	500	477.84	3.6×10^{-5}	94.73

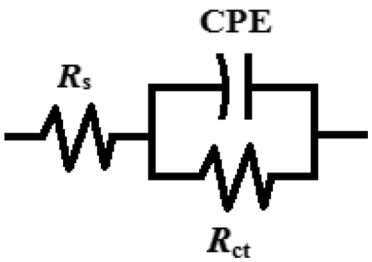

Fig. 6 Equivalent circuit of constant phase element (CPE)

molecules by adsorption of inhibitor on low carbon steel surface, lessening the degree of metal disintegration. The only one peak for individual concentration of inhibitor in Bode plots shows that the OCP was well set with time. Again the magnitude of impedance at 100 mg/L to 500 mg/L increases as compared to the blank solution which shows the inhibition effect of the inhibitor.

3.5 FTIR Analysis

The presence of the heteroatoms in natural products may help the adsorption of the inhibitor molecules on steel surface to inhibit the corrosion of low carbon steel [41, 42]. In the present work, the FTIR spectroscopy was utilized to confirm existence of heteroatoms containing functional groups in the extract. The FTIR spectra of the *C. sinensis* extract are shown in Fig. 7. The FTIR spectra of the *C. sinensis*

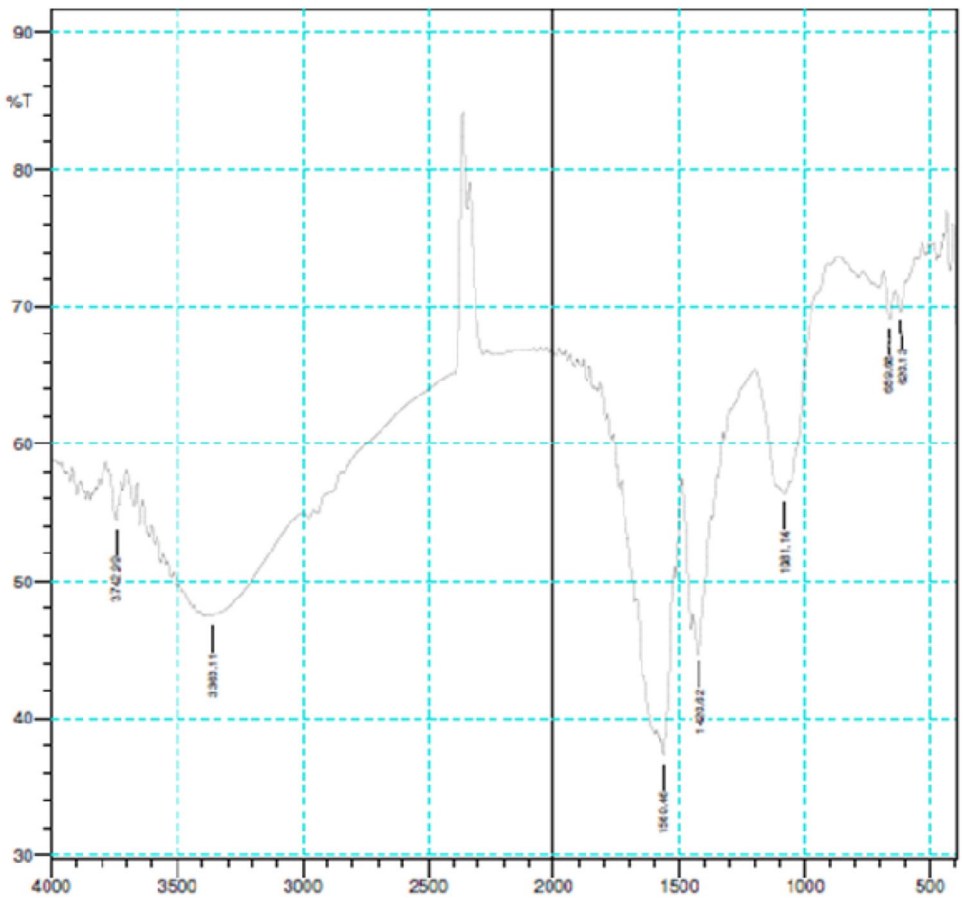

Fig. 7 FTIR spectrum of *C. sinensis* extract

Table 6 FTIR data of *C. sinensis* extract

S. No.	Wavenumber (cm^{-1})	Functional group
1.	3343.11	O–H stretching
2.	1504.40	C–O stretching
3.	1091.14	Aromatic ring

extract show the existence of the functional groups, which is reported in the Table 6. The outcomes from FTIR analysis show that the *C. sinensis* extract has anti-corrosive activities due to the presence of heteroatoms.

3.6 UV–Visible Spectroscopy

The UV spectra of the *C. sinensis* extract before and after the corrosion test were taken and they are shown in Fig. 8. From the UV spectra, the absorbance of the corrosive medium before the corrosion test is higher than the absorbance of corrosive medium after the corrosion test. It simply shows that, when the low carbon steel sample was immersed into the acidic solution of *C. sinensis* extract, some molecules from the solution have been adsorbed on the metal surface [5]. The value of the absorption maximum (λ_{max}) or a change in the value of absorbance recommended the formation of a complex between the steel surface and inhibitor molecules.

3.7 Surface Studies

The SEM and AFM images of non-corroded, corroded, and the inhibited low carbon steel coupons are shown in Fig. 9. These SEM and AFM images were compared. The surface of non-corroded mild steel seems to be absolutely fine, but we observed severely harmed surface for the corroded mild steel. It happened because the low carbon steel was immersed in the corrosive medium and the surface gets corroded and for the inhibited steel coupon; the surface is comparatively improved because of the adsorption of the inhibitor.

The AFM studies provide the value of surface roughness. The surface roughness of non-corroded, corroded and the inhibited low carbon steel are 2.099 nm, 138.807 nm, and 34.15 nm, respectively. The increase in surface roughness of low carbon steel is because of the contact of metal with the corrosive medium while the surface roughness decreases for inhibited steel coupon showing the adsorption of inhibitor. This decrease is surface roughness is because of the formation of a protective layer on the metal surface because of the adsorption of *C. sinensis* extract on the surface of the low carbon steel.

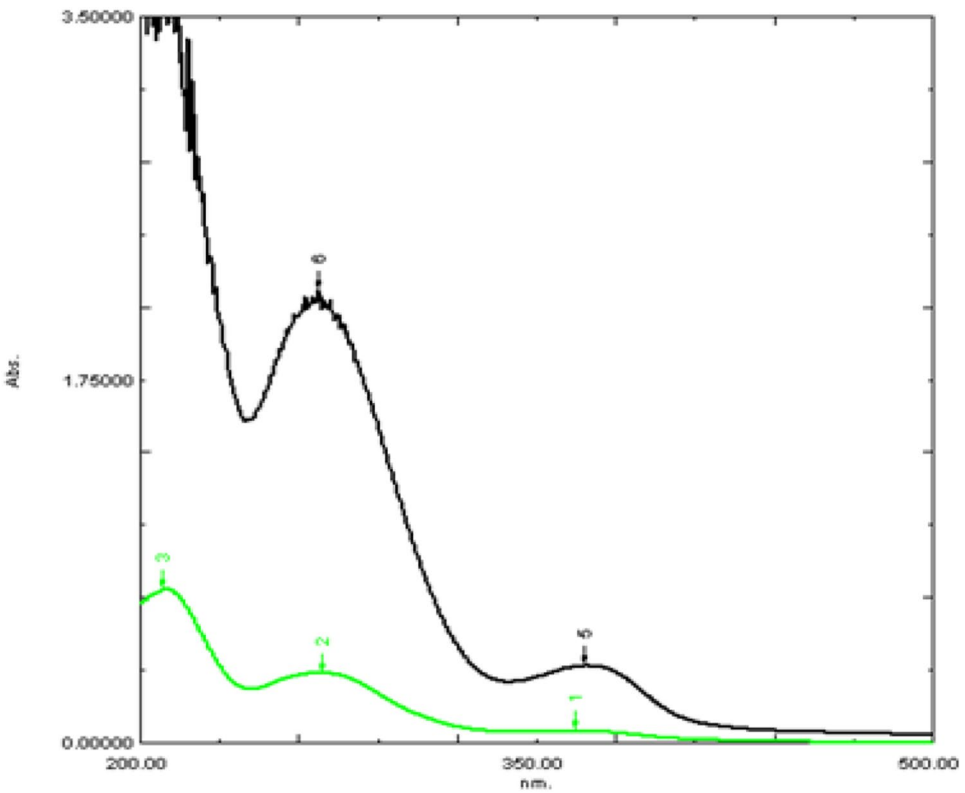

Fig. 8 UV Spectra of *C. sinensis* extract before and after the corrosion test

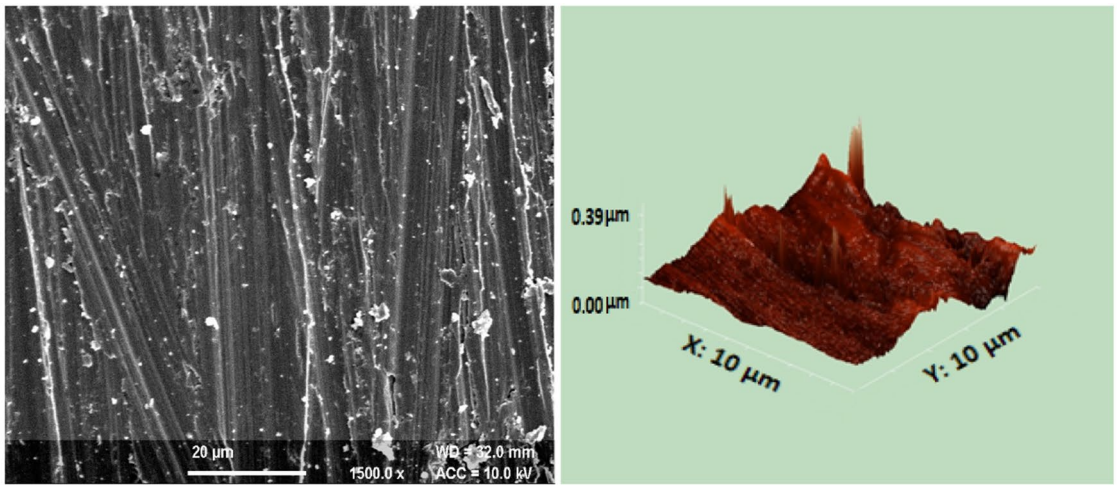

Non-corroded low carbon steel

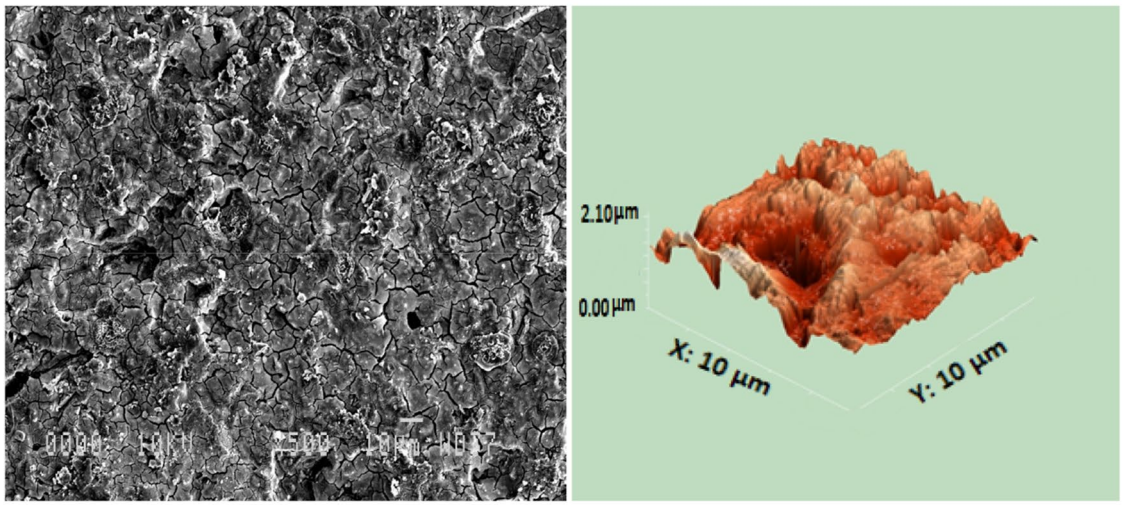

Corroded low carbon steel immersed in 0.5 M H_2SO_4

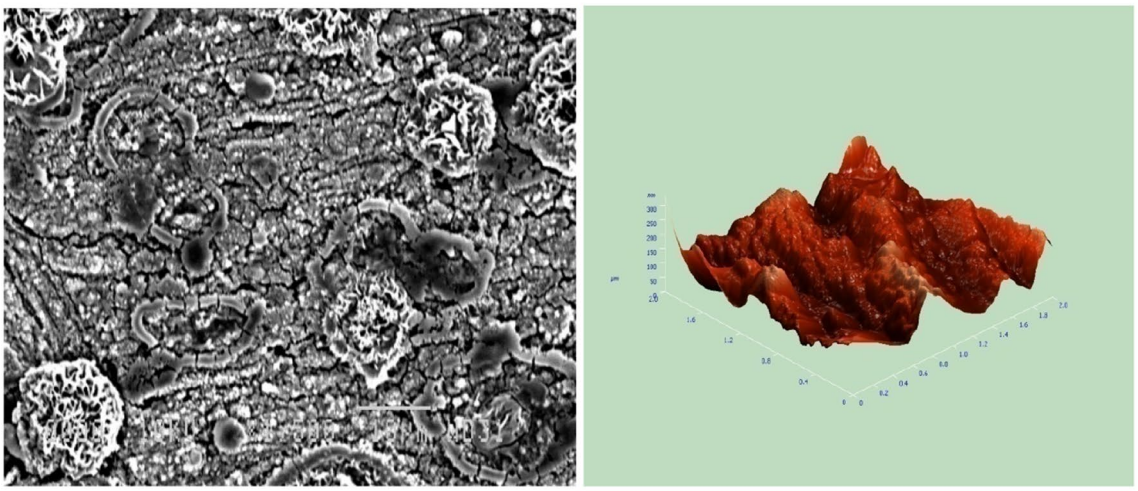

Inhibited low carbon steel

Fig. 9 SEM and AFM images of non-corroded, corroded and inhibited low carbon steel

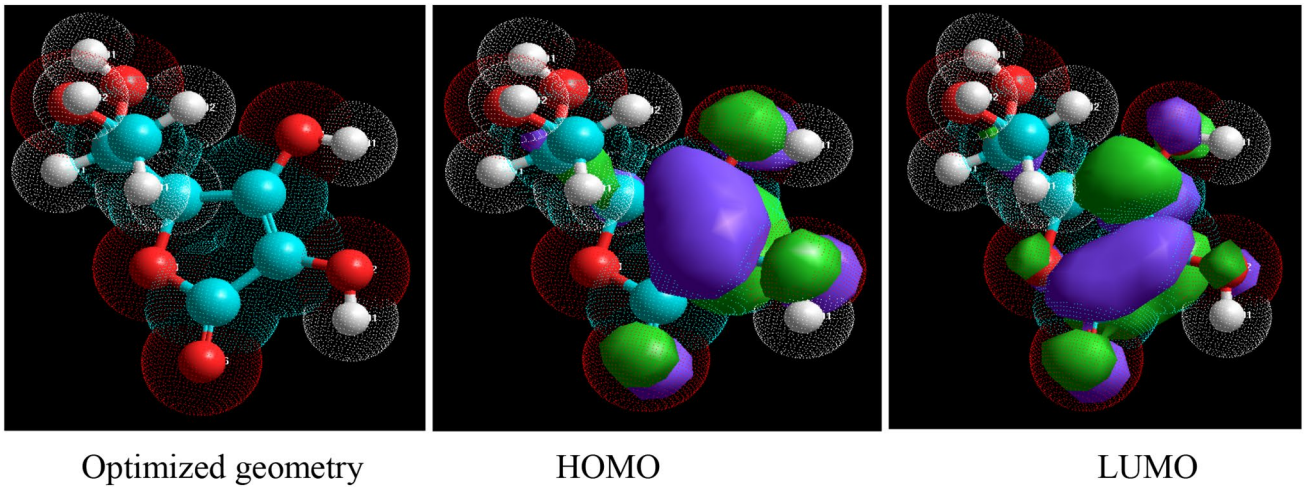

Fig. 10 Optimization geometry of Ascorbic acid with HOMO and LUMO density

3.8 Quantum Chemical Calculation

Using the Hyperchem 8.0 software, the HOMO and LUMO orbitals of the Ascorbic acid were drawn and the energy of these orbitals was determined. These orbitals are shown in Fig. 10 and the energy difference, the energy of HOMO and LUMO are reported in Table 7. The smaller be the energy gap between the HOMO and LUMO, stronger will be the adsorption of the inhibitor.

4 Conclusion

After conducting several experiments based on weight reduction, electrochemical analysis, and the surface morphology, it is observed that-

- The results of weight reduction experiments and electrochemical analysis are in good agreement i.e., both are in favor of the advancement of inhibition capacity of the inhibitor on moving to the higher concentrations.
- Both the SEM and AFM studies strongly favor the development of a protective layer on low carbon steel on applying the *C. sinensis* extract.
- The present inhibitor can be considered as a combine type inhibitor for low carbon steel.

Table 7 Quantum Chemical Parameters for the chemical constituent of *C. sinensis*

S. No/	Parameter	Ascorbic acid
1/	E_{HOMO} (ev)	−9.5898
2/	E_{LUMO} (ev)	−0.4296
3/	ΔE (ev)	−9.1602

Compliance with Ethical Standards

Conflict of interest There is no conflict of interest.

References

1. Jacob K, Parameswaran G (2010) Corrosion inhibition of mild steel in hydrochloric acid solution by Schiff base furoin thiosemicarbazone. Corros Sci 52:224–228
2. Wahadan M, Hermas A, Morad M (2002) Corrosion inhibition of carbon-steels by propargyl triphenyl phosphonium bromide in H_2SO_4 solution. Mater Chem Phys 76:111–118
3. Sapre K, Seal S, Jepson P, Wang H, Rahman Z, Smith T (2003) Investigation into the evolution of corrosion product layer (CPL) of 1018 C-steel exposed to multiphase environment using FIB and EIS techniques. Corros Sci 45:59–80
4. Njoku D, Ukaga I, Ikenna O, Oguzie E, Oguzie K, Ibisi N (2016) Natural products for materials protection: corrosion protection of aluminium in hydrochloric acid by *Kola nitida* extract. J Mol Liq 219:417–424
5. Okafor P, Ikpi M, Uwah I, Ebenso E, Ekpe U, Umoren S (2008) Inhibitory action of Phyllanthus amarus extract on the corrosion of mild steel in acidic media. Corros Sci 50:2310–2317
6. Noor E (2011) The impact of some factors on the inhibitory action of Radish seeds aqueous extract for mild steel corrosion in 1 M H_2SO_4 solution. Mater Chem Phys 131:160–169
7. Rajeswari V, Kesavan D, Gopiraman M, Viswanathamurthi P, Poonkuzhali K, Palvannan T (2014) Corrosion inhibition of *Eleusine aegyptiaca* and *Croton rottleri* leaf extracts on cast iron surface in 1 M HCl medium. Appl Surf Sci 314:537–545

8. Hamdy A, El-Gendy NSh (2013) Thermodynamic, adsorption and electrochemical studies for corrosion inhibition of carbon steel by *henna* extract in acid medium. Egypt J Petr 22:17–25
9. Kalaiselvi P, Chellammal S, Palanichamy S, Subramanian G (2010) Artemisia pallens as corrosion inhibitor for mild steel in HCl medium. Mater Chem Phys 120:643–648
10. Rahim A, Rocca E, Steinmetz J, Kassim M, Adnan R, Ibrahim M (2007) Mangrove tannins and their flavonoid monomers as alternative steel corrosion inhibitors in acidic medium. Corros Sci 49:402–417
11. Soltani N, Tavakkoli N, Khayatkashani M, Jalali M, Mosavizade A (2012) Green approach to corrosion inhibition of 304 stainless steel in hydrochloric acid solution by the extract of *Salvia officinalis* leaves. Corros Sci 62:122–135
12. Anupama KK, Ramya K, Shainy KM, Joseph A (2015) Adsorption and electrochemical studies of *Pimenta dioica* leaf extracts as corrosion inhibitor for mild steel in hydrochloric acid. Mater Chem Phys 167:28–41
13. Odewunmi N, Umoren SA, Gasem Z (2013) Utilization of *watermelon* rind extract as a green corrosion inhibitor for mild steel in acidic media. J Ind Eng Chem 21:239–247
14. Raja PB, Qureshi A, Rahim A, Osman H, Awang K (2013) Neolamarckia cadamba alkaloids as eco-friendly corrosion inhibitors for mild steel in 1 M HCl media. Corros Sci 69:292–301
15. Obi-Egbedi N, Obot I, Umoren S (2012) *Spondias mombin* L. as a green corrosion inhibitor for aluminium in sulphuric acid: correlation between inhibitive effect and electronic properties of extracts major constituents using density functional theory. Arab J Chem 5:361–373
16. Li X, Deng S, Fu H (2012) Inhibition of the corrosion of steel in HCl, H_2SO_4 solutions by *bamboo* leaf extract. Corros Sci 62:163–175
17. Rho M, Lee S, Park H, Choi J, Kang J, Kim K, Lee H, Kim Y (2007) ACAT inhibition of alkamides identified in the fruits of *Piper nigrum*. Phytochemistry 68:899–903
18. Sorkhabi H, Haghi M (2009) Corrosion inhibition of mild steel in hydrochloric acid by betanin as a green inhibitor. J Solid State Electrochem 13:1297–1301
19. Hegazy M, Altam F (2016) Three novel *bola amphiphiles* as corrosion inhibitors for carbon steel in hydrochloric acid: experimental and computational studies. J Mol Liq 218:649–662
20. Singh D, Kumar S, Udayabhanu G, John R (2016) 4(N, N-dimethylamino) benzaldehyde nicotinic hydrazone as corrosion inhibitor for mild steel in 1 M HCl solution: an experimental and theoretical study. J Mol Liq 216:738–746
21. Seiverts A, Lueg P (1923) Anog Chem 126:192
22. Cheng S, Chen S, Liu T, Chang X, Yin Y (2007) Carboxymethyl *chitosan* as an ecofriendly inhibitor for mild steel in 1 M HCl. Mater Lett 61:3276–3280
23. Murulana L, Kabanda M, Ebenso E (2016) Investigation of the adsorption characteristics of some selected sulphonamide derivatives as corrosion inhibitors at mild steel/hydrochloric acid interface: experimental, quantum chemical and QSAR studies. J Mol Liq 215:763–779
24. Liao L, Mo S, Luo H, Li N (2016) Longan seed and peel as environmentally friendly corrosion inhibitor for mild steel in acid solution: experimental and theoretical studies. J Colloid Interface Sci 499:110–119
25. Lgaz H, Salghi R, Jodeh S, Hammout B (2016) Effect of clozapine on inhibition of mild steel corrosion in 1.0 M HCl medium. J Mol Liquids 225:271–280
26. Raja P, Quraishi A, Rahim A, Osman H, Awang K (2013) *Neolamarckia cadamba* alkaloids as eco-friendly corrosion inhibitors for mild steel in 1 M HCl media. Corros Sci 69:292–301
27. Nofrizal S, Rahim A, Saad B, Raja P, Shah M, Yahya S (2011) Elucidation of the corrosion inhibition of mild steel in 1.0 M HCl by catechin monomers from commercial green tea extracts. Metall Mater Trans A. https://doi.org/10.1007/s11661-011-1030-3
28. Junaedi S, Amiery A, Kadihum A, Kadhum A, Mohamad A (2013) Inhibition effects of a synthesized novel 4-aminoantipyrine derivative on the corrosion of mild steel in hydrochloric acid solution together with quantum chemical studies. Int J Mol Sci 14:11915–11928
29. Saxena A, Prasad D, Haldhar R, Singh G, Kumar A (2018) Use of *Saraca ashoka* extract as green corrosion inhibitor for mild steel in 0.5 M H_2SO_4. J Mol Liq 258:89–97
30. Piracha N, Ito F, Nakanaga T (2004) Infrared depletion spectroscopy of aniline–toluene cluster: the investigation of the red shifts of the NH2 stretching vibrations of aniline–aromatic clusters. Chem Phys 297:133–138
31. Chetouani A, Hammouti B, Benhadda T, Daudi M (2005) Inhibitive action of bipyrazolic type organic compounds towards corrosion of pure iron in acidic media. Appl Surf Sci 249:375–385
32. Unterberg C, Gerlach A, Jansen A, Gerhards M (2004) Structures and vibrations of neutral and cationic 3- and 4-aminophenol. Chem Phys 304:237–244
33. Saranya J, Sounthari P, Parameswari K, Chitra S (2016) Acenaphtho [1,2-b] quinoxaline and Acenaphtho [1,2-b]pyrazine as corrosion inhibitors for mild steel in acid medium. Meas J Int Meas Confed 77:175–185
34. Ramezanzadeh B, Vakili H, Amini R (2015) The effects of addition of poly(vinyl) alcohol (PVA) as a green corrosion inhibitor to the phosphate conversion coating on the anticorrosion and adhesion properties of the epoxy coating on the steel substrate. Appl Surf Sci 327:174–181
35. Singh M, Bhrara K, Singh G (2008) The inhibitory effect of diethanolamine on corrosion of mild steel in 0.5 M sulphuric acidic medium. Port Electrochim Acta 6:479–492
36. Achary G, Naik Y, Kumar S, Venkatesha T, Sherigara B (2008) An electroactive co-polymer as corrosion inhibitor for steel in sulphuric acid medium. Appl Surf Sci 254:5569–5573
37. Singh P, Srivastava V, Quraishi M (2016) Novel quinoline derivatives as green corrosion inhibitors for mild steel in acidic medium: electrochemical, SEM, AFM, and XPS studies. J Mol Liq 216:164–173
38. Cruz J, Pandiyan T, Ochoa E (2005) A new inhibitor for mild carbon steel: electrochemical and DFT studies. J Electroanal Chem 583:8–16
39. Khadraoui A, Khelifa A, Hadjmeliani M, Mehdaoui R, Hachama K, Tidu A, Azari Z, Obot I, Zarrouk A (2016) Extraction, characterization and anti-corrosion activity of *Mentha pulegium* oil: weight loss, electrochemical, thermodynamic and surface studies. J Mol Liq 216:724–731
40. Saxena A, Prasad D, Haldhar R (2018) Investigation of corrosion inhibition effect and adsorption activities of *Cuscuta reflexa* extract for mild steel in 0.5 M H_2SO_4. Bioelectrochemistry 124:156–164
41. Raja P, Quraishi A, Rahim A, Osman H, Awang K (2013) "*Neolamarckia cadamba* alkaloids as eco-friendly corrosion inhibitor for mild steel in 1 M HCl media. Corros Sci 69:292–301
42. Satapathy A, Gunasekaran G, Sahoo S, Kumar A, Rodrigues P (2009) Corrosion inhibition by *Justicia gendarussa* plant extract in hydrochloric acid solution. Corros Sci 51:2848–2856